JOURNAL OF SOLID STATE CHEMISTRY **126,** 169–176 (1996)
ARTICLE NO. 0325

# Synthetic Pathways for New Tubular Transition Metal Hydroxo- and Fluoro-Selenites: Crystal Structures of $M_{12}(X)_2(SeO_3)_8(OH)_6$ ($M = Co^{2+}$, $Ni^{2+}$; $X = OH^-$)

Pedro Amorós,[1] M. Dolores Marcos, Manuel Roca, Aurelio Beltrán-Porter, and Daniel Beltrán-Porter

*UIBCM, Departament de Química Inorgànica, Facultat de Químiques, and Institut Universitari de Ciència dels Materials, Universitat de València, Dr. Moliner 50, 46100-Burjassot (València), Spain*

Received March 13, 1996; in revised form June 19, 1996; accepted June 26, 1996

**The dumortierite-family structures $M_{12}X_2(SeO_3)_8(OH)_6$ ($M = Co^{2+}$ and $Ni^{2+}$; $X = OH^-$ and $F^-$) have been synthesized. The crystal structures of the hydroxo-derivatives have been refined from X-ray powder diffraction data in the space group $P6_3mc$ ($Z = 1$) with $a = 12.887(3)$ Å and $c = 4.981(4)$ Å ($M = Co^{2+}$, $X = OH^-$ or $F^-$) and $a = 12.704(5)$ Å and $c = 4.925(6)$ Å ($M = Ni^{2+}$, $X = OH^-$ or $F^-$). Application of the Partial Charge Transference Model allows the understanding of the selenite derivatives crystal chemistry.** 

## INTRODUCTION

The formation of microporous phosphates is currently of considerable interest because a number of them display useful properties as catalysts, sorbents, and ionic exchangers (1, 2). In contrast, the chemistry of selenium oxysalts is less well known (3, 4). Se(IV) has a stereochemically active lone pair of electrons and has pyramidal geometry with three (oxygen) ligands. The lone pair of electrons ($E$) occupies the fourth coordination position in the pseudo-tetrahedral $ESeO_3^{2-}$ group (5–7). There are few well-defined structural families of selenites, but a number of compounds in the Co/Ni–Se–O system have been characterized (8–15).

We have recently advanced a systematic strategy of soft-chemistry synthesis of frameworks isostructural with dumortierite (17): $M_{12}Z_nT_8(OH)_6$ ($M$ = transition metal, $T$ = tetrahedral or pseudo-tetrahedral species, $Z$ = cation or anion species required to balance the charge). Several isostructural solids have been described: $M_{11}\square(HPO_3)_8(OH)_6$ ($M = Zn^{2+}$ (18), $Co^{2+}$, $Ni^{2+}$ (19), $Fe^{2+}$, $Mn^{2+}$ (20)), $M_{12+x}H_{6-2x}(AO_4)_8(OH)_6$ ($M = Co^{2+}$, $Ni^{2+}$; $A$ = P (17, 21), As (22)), and $M_{12}(TeO_3)_8(OH)_8$ ($M = Co^{2+}$, $Ni^{2+}$) (23). The present paper describes the synthesis and crystal structures of the new hydroxo- and fluoro-selenites $M_{12}(X)_2(SeO_3)_8(OH)_6$ ($M = Co^{2+}$, $Ni^{2+}$; $X = OH^-$, $F^-$) of the dumortierite family. In addition, dealing with the preparative strategy, we intend to show how a simple model, the Progressive Charge Transference Model (PCTM) (24), allows us to understand the preparative and crystal chemistry of the $M$–Se–O system.

## EXPERIMENTAL

### *Synthesis*

The synthesis procedure is similar to that described in Ref. (17). Polycrystalline samples of $Ni_{12}(OH)_2(SeO_3)_8(OH)_6$ were prepared from direct reaction of $NiCl_2 \cdot 6H_2O$ and $SeO_2$. $NiCl_2 \cdot 6H_2O$ (3.948 g, 16.6 mmol) was dissolved in 7 ml of water. Over this solution 6 ml of 1.4 $M$ KOH was dripped and a pale green suspension of pH *ca.* 6 was obtained. The selenite solution was prepared by neutralization (until pH 6) of a solution containing 1.243 g (11.2 mmol) of $SeO_2$ in 20 ml of water with 1.4 $M$ KOH. Then, this last solution was added to the nickel suspension with stirring, and the mixture was placed in a Teflon bomb filled to 90% of its volume and heated, under autogeneous pressure, at 180°C over a week. The solid was filtered, washed with water and acetone, and air dried. A very fine pale-green polycrystalline powder was obtained (Anal: found, Ni 37.2% and Se 34.3%. Required, Ni 37.9% and Se 34.8%).

The cobalt derivative, $Co_{12}(OH)_2(SeO_3)_8(OH)_6$, was prepared in a similar way starting from 3.948 g (16.6 mmol) of $CoCl_2 \cdot 6H_2O$ and 1.243 g (11.2 mmol) of $SeO_2$. The resulting mixture was handled as above. A very fine violet polycrystalline precipitate was separated by filtration, washed with water and acetone, and air dried (Anal: found, Co 38.3% and Se 34.4%. Required, Co 38.0% and Se 34.0%).

The hydroxo-fluoro-selenites, $M_{12}(F)_2(SeO_3)_8(OH)_6$ ($M = Co^{2+}$, $Ni^{2+}$), were obtained by adding 1 g of NaF (23.8 mmol) in 5 ml of distilled water to the metal suspension at pH *ca. 6*. The selenite solution and the reaction conditions were exactly as above. The solids were filtered, washed with water and acetone, and air dried (Anal. Co-derivative:

[1] To whom correspondence should be addressed.



0022-4596/96 $18.00

found, Co 38.0%, Se 33.9%, F 2.0%. Required, Co 37.8%, Se 34.2%, F 1.9%. Ni derivative: found, Ni 37.5%, Se 34.3%, F 2.2%. Required, Ni 37.9%, Se 34.0%, F 2.0%).

A complementary set of experiments modifying the pH conditions was also done. As previously shown for related cases (17), very different solids might be isolated by altering the hydrolytic and condensation processes involving the metal cations. Thus, strict control of this variable is required to gain insight on the chemistry of the *M*–Se–O systems.

### *Analysis and Physical Measurements*

Ni, Co, Se, and F contents in the respective derivatives were determined, after dissolution of the solids in boiling concentrated hydrochloric acid, by atomic absorption spectrometry (Perkin–Elmer Zeeman 5000). IR spectra (KBr pellets) were recorded on a Perkin–Elmer 882 infrared spectrophotometer. Thermal studies were performed using a Perkin–Elmer TGA-7 analyzer.

### *X-Ray Data*

X-ray powder diffraction data were obtained with a Siemens D501 automated diffractometer using graphite-monochromatized Cu$K\alpha$ radiation. $Pb(NO_3)_2$ was used as the internal standard when data for indexation purposes were collected. In these cases the patterns were scanned in steps of 0.02°($2\theta$) over the angular range 5°–70°($2\theta$) for 8 s per step. The TREOR (25) and LSUCRE (26) programs were used to index and refine the cell parameters, respectively. For Rietveld analysis, the X-ray powder data were collected with the same scan-step interval (0.02°($2\theta$)), but a wider $2\theta$ angular range (5°–110°($2\theta$)) and a longer acquisition time (18 s per step) were used to enhance statistics.

The refinements were done with GSAS (27) using a pseudo-Voigt peak function corrected for asymmetry at low angles; a refined background function was used in the analysis.

## RESULTS AND DISCUSSION

### *Strategy of Synthesis*

Traditional solid-state synthesis techniques for highly condensed materials involve treatment at high temperature and pressure. Indeed, the first compounds in the dumortierite family were synthesized from transition metal and tellurium oxides under hydrothermal conditions ($T$ = 380°C, $P$ = 900 bar) (23). In these reactions, the mechanism of reaction is generally not considered and there is no control over the formation of metastable intermediate precursors. In contrast, the most important aspect of the procedure reported here lies in the systematic and reproducible synthesis of condensed selenites using soft-chemistry techniques involving retention of structural elements of reactants or intermediate precursors in the final solid.

Our synthesis approach is based on a very simple idea: the resulting framework in the final solid is affected by the species present in the mother solution. The role of the anionic species varies, depending on the condensation degree of the cationic species; two extreme cases can be discussed. First, at low pH values, the cationic condensations very low prior to the nonaqueous ligand addition, and the role played by the nonaqueous bridge oxoligands strongly affects the final packing. At higher pH values, higher connectivity of the cationic species exists due to their hydrolysis and condensation processes, and the influence of the nonaqueous bridging ligands on the final framework structure decreases. Hence, pH and metal concentration control the hydrolysis and subsequent condensation processes, and hence control the isolation of solids containing more or less complex cation clusters.

At low pH values (low hydrolysis and low condensation of metallic cations), $M(H_2O)_6^{2+}$ are the predominant species. Consequently, OH groups are not expected in the structure of the resulting solids (28) and low-condensed materials will be obtained. For the selenite oxyanions, the resulting solids $M_3(SeO_3)_3 \cdot H_2O$ ($M = Co^{2+}, Ni^{2+}$) (11, 12) have octahedra linked only by $SeO_3^{2-}$ anions. For other tetrahedral oxoanions ($HPO_3^{2-}$ or $PO_4^{3-}$), the same situation occurs. For example, dealing with the phosphite derivatives, it is possible to isolate $M(HPO_3) \cdot H_2O$ ($M = Co^{2+}$, $Ni^{2+}$) (30, 31); for phosphate anions, the solids $M_7(PO_4)_2(HPO_4)_4$ (32) are obtained.

The fact that the solids isolated at low pH values show very different structures, depending on the anion involved, is consistent with our synthesis approach: when no cation condensation is present in the mother solution, the bridging oxoanions govern the connectivity in the final solid. Hence, the reaction mechanism at low pH values is of the solution-mediated transport type. The reagents are dissolved in the reaction medium and there is not any cationic precursor involving preformed units for solid building present.

In contrast, under the conditions of synthesis for the title compounds, the existence of OH-containing cationic aggregates reduces the possible bridging modes in which the different anions could act, and allows us to obtain a wide family of isostructural solids. Synthesis of all members of the dumortierite family can be considered as governed by a solid-hydrogel transformation mechanism. In every case, a solid hydroxo-metallic precursor is obtained prior to the addition of the oxoanionic ligand. This precursor could be thought of as a polymer formed from the predominant species in the solution ($M_2(OH)^{3+}$, $M = Co^{2+}$, $Ni^{2+}$ (33)) in which the characteristic double chains of the dumortierite-like solids might already be formed. The addition of the pseudo-tetrahedral oxoanionic species complete the condensation process and the temperature and pressure required for the isolation of these tubular materials

(soft hydrothermal synthesis) are only necessary in order to improve the crystallinity of the resulting product.

The members of this family were synthesized in a very similar way, adjusting the general synthetic conditions for each case. For the fluoro-selenites $M_{12}(F)_2(SeO_3)_8(OH)_6$ ($M = Co^{2+}$, $Ni^{2+}$), a high $F^-$ concentration in the medium was necessary to displace the $OH^-$ groups which act as guest species in the hexagonal channels in $M_{12}(SeO_3)_8(OH)_8$. The synthesis of other halogen-selenites was unsuccessful due to structural impediments (see below). In the synthesis of the Se-containing derivatives, control of the pH of the reaction mixture is particularly important in order to prevent the reduction of $SeO_2$ to Se metal. According to the Pourbaix diagram (34), the pH range for the $SeO_3^{2-}$ anions is from 2.5 to 6.5, in which the proposed synthesis procedure takes place.

## APPLICATION OF THE PROGRESSIVE CHARGE TRANSFERENCE MODEL

The PCTM (24) helps us to understand the crystal chemistry of this system. Following the PCTM ideas, the formation of selenite derivatives can be viewed as the result of the formal competition between $H_2O$ molecules (coordinated to the cation species previously existing in the solution) and selenite ligands. To summarize this model (25), (a) the metal–ligand interactions are considered as electrostatic, (b) the net anionic charge is symmetrically distributed, (c) a formally progressive substitution of $H_2O$ molecules in the metal coordination sphere is assumed, (d) the incoming anions supply the cation with the maximum charge-fraction carried by one terminal donor atom, and (e) covalence effects promote *cis*-substituted arrangements. We summarize (Fig. 1) the different bridging modes in which selenite anions may be involved, and the most important octahedra in relation to selenite anions for divalent transition metals (Fig. 2).

The minimum coordination expected for selenite anions ($SeO_3^{2-}$) is represented as mode I (Fig. 1), in which each anion can coordinate three different metal centers (*i.e.*, the formal charge on each oxygen atom should be 2/3). For acid-selenites, the minimum coordination (Fig. 1, mode V) implies donation of a formal charge of 1/2 through each one of the two donor oxygen atoms to a maximum of two different metal cations. If we consider now the coordination of these polyhedra by divalent cations, the charge compensation will require ligand-to-metal ratios of 2 for $HSeO_3^-$ and 1 for $SeO_3^{2-}$. Hence, the maximum direct charge transfer from each donor atom (minimum coordination number) implies four oxygen donor atoms from $HSeO_3^-$ anions (mode V) and three from $SeO_3^{2-}$ anions (mode I). Thus, it might be expected that acid-selenites and selenites of divalent transition metals crystallize in dilute acid media with two (Fig. 2, *B* polyhedron) and three (Fig. 2, *A* polyhedron) $H_2O$ molecules in the cation coordination sphere, respectively. The isolation of solids having lower hydration states is possible by varying the experimental conditions. $H_2O$ may be eliminated as ligands by increasing the crystallization temperature and limiting the presence of water in the reaction medium. This is the case for the hydrothermal procedures commonly used to obtain selenite derivatives.

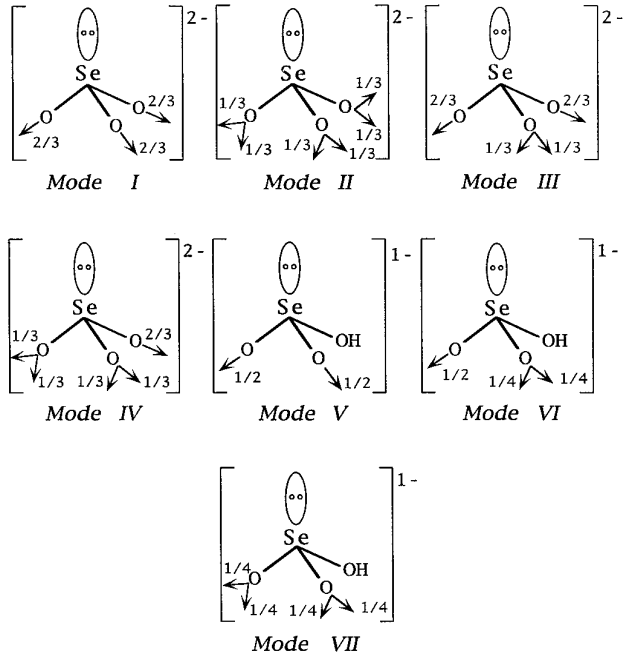


**FIG. 1.** Schematic representation of some coordination modes in which selenite ($SeO_3^{2-}$) and hydrogenselenite ($HSeO_3^-$) anions may be involved.

In order to maintain charge balance, any decrease in the hydration state implies an increase in the number of metal cations to which each anion must link. Hence, some of the donor oxygen atoms will be shared by two cations (modes II to IV for selenite and VI and VII for acid-selenites), leading to an increase in the condensation of the cation polyhedra in the final material.

In order to corroborate validity of the model, we have applied the PCTM to selected solids. For $K_2Co(SeO_3)_2$ (15), if we consider the hypothetical anion $[Co(SeO_3)_2]^{2-}$, the Co octahedra involves six oxygen atoms belonging to $SeO_3^{2-}$ groups, which transfer a $-2/3$ formal charge to the metal center. The bridging mode I for $SeO_3^{2-}$ anions and the type *C* isolated polyhedra (Fig. 2) for Co atoms are predicted. In fact, the structure shows the existence of $CoO_6$ octahedra only connected through $\mu$(O,O′)selenite bridges. For $K_2Co_2(SeO_3)_3$ (35), the formal anion $[Co_2(SeO_3)_3]^{2-}$ can be considered, and there is a formal residual charge of $-1$ for each cobalt atom. The PCTM predicts highly condensed polyhedra of type *D* (Fig. 2) which, in

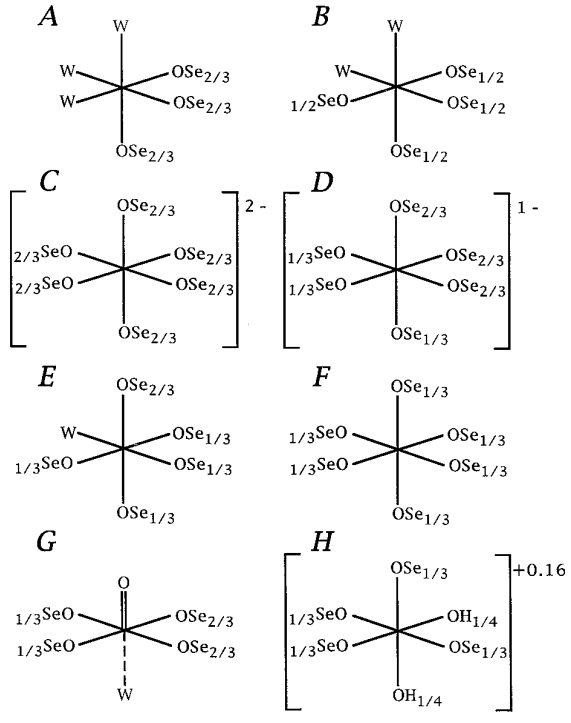


**FIG. 2.** Some types of transition metal cationic polyhedra found in selenite derivatives. $W$ = coordinated water molecules. $OSe_{2/3}$ = $\mu$-(O,O′)–$SO_3^{2-}$ bridges. $OSe_{1/3}$ = $\mu$-(O)–$SeO_3^{2-}$ bridges. $OSe_{1/2}$ = $\mu$-(O,O′)–$HSeO_3^-$ bridges. $OH_{1/4}$ = $\mu$-(O)–hydroxo bridges connecting four metal atoms.

this case, corresponds to face-sharing dimers. Solid $Ni_3(SeO_3)_3 \cdot H_2O$ (11, 12) shows a very complex structure. If we consider that the $H_2O$ molecule is coordinated to one of the three nickel atoms per formula unit, two different metal polyhedra, of type *E* and *F* (see Fig. 2), are proposed by the PCTM, and hence this solid will present a high Ni octahedra connectivity.

On the other hand, peculiarities of the cations can result in coordination polyhedra very different from those discussed so far. This is the case of the highly anisotropic oxovanadium $VO^{2+}$ ion, present in the solid $VOSeO_3 \cdot H_2O$ (5). Normally, the oxygen atom of the $VO^{2+}$ group cannot be substituted and the large V–O distance, *trans* to the V=O bond, is inadequate for effective charge transfer. The result is the typical 1 + 4 + 1 coordination observed in most oxovanadium compounds and type *G* polyhedra are predicted (see Fig. 2). This type of polyhedra could give rise to zigzag corner-sharing chains of metal octahedra or, as in the case of $VOSeO_3 \cdot H_2O$, to an edge-sharing dimer.

Finally, when the synthesis is done at higher pH (*ca.* 6), as in the case of the title compounds, hexaquo-cations are not the predominant species in solution. The reaction can be thought of as starting from a hydroxo-polymer obtained from the cation cluster $M_2(OH)^{3+}$, one of the dominant species in solution under these experimental conditions (28). If this polymer forms because of the nucleofilic character of OH group in the $M_2(OH)^{3+}$ species, the charge involved in each $M$–OH bond should be 1/4. Taking into account the stoichiometry of the formal ion $[M_{12}(SeO_3)_8(OH)_6]^{2+}$, which constitutes the covalent framework of the title compounds, a polyhedra of the *H* type (Fig. 2) can be predicted, in accord with the structural data.

### *Structure Refinement of $M_{12}(OH)_2(SeO_3)_8(OH)_6$ ($M$ = $Co^{2+}$, $Ni^{2+}$)*

Lattice constants were calculated from the positions of 25 accurately measured reflections. Hexagonal cells with $a$ = 12.887(3) Å and $c$ = 4.981(4) Å ($M$ = $Co^{2+}$) and $a$ = 12.704(5) Å and $c$ = 4.925(6) Å ($M$ = $Ni^{2+}$) were obtained. These cells are very close to those previously reported for the other dumortierite-like solids; systematic absences also are consistent with the space group $P6_3mc$. Rietveld refinements were initiated in this space group using the atomic parameters of the telluride derivative $Co_6(TeO_3)_4(OH)_4$ (23) as the starting model. In the final refinements, a total of 32 parameters (16 positional parameters, 3 isotropic displacement parameters, 5 profile coefficients, and 6 background terms) were refined in each case. For the Co derivative an empirical absorption correction was applied. For the Ni derivative the largely asymmetric (100) and (010) reflections were omitted and two excluded regions were considered (due to the presence of a small amount of an unknown phase, probably $NiSe_2O_5$ (13)). Conventional reliability factors, final profile, and structural parameters are gathered in Table 1 for the cobalt and nickel derivatives. Dealing with standard deviations, several authors conclude that the Rietveld method probably underestimates systematically the statistical dispersions, this problem increasing when small step width and long step counting time are used (36, 37). To avoid this problem, a simple calculation proposed by Berar and Lelann (38), which takes into account local correlations, has been applied to furnish a more reliable estimate of the e.s.d. values. Accordingly, to obtain realistic e.s.d. values, the mathematical values given in Table 1 should be multiplied by the factors at the foot of this table. Calculated and observed profiles are shown in Figs. 3 and 4. Selected bond distances and angles are given in Table 2.

### *Description of the Structure*

The structure of $M_{12}(OH)_2(SeO_3)_8(OH)_6$ ($M$ = $Co^{2+}$, $Ni^{2+}$) is shown in Fig. 5. These two new selenite derivatives are isostructural with the tellurites $M_3(TeO_3)_2(OH)_2$ ($M$ = $Co^{2+}$, $Ni^{2+}$) (23) and belong to the dumortierite structural

**TABLE 1**
**Final Profile and Structural Parameters for $M_{12}(OH)_2(SeO_3)_8(OH)_6$ ($M = Co^{2+}$, $Ni^{2+}$) in Space Group $P6_3mc$, and Cell Parameters of $M_{12}(F)_2(SeO_3)_8(OH)_6$ ($M = Co^{2+}$, $Ni^{2+}$)**

$M = Co^{2+}$; $X = OH^-$

| Cell data | | Reliability factors (%) | |
|---|---|---|---|
| $a = 12.8893(2)$ Å | $V = 716.42(3)$ Å$^3$ | $R_{wp} = 5.89$ | $R_p = 4.46$ $R_B = 2.47$ |
| $c = 4.9794(1)$ Å | $Z = 1$ | $\chi^2 = 2.06$ | |

| Atom | Site | Occupancy | $x/a$ | $y/b$ | $z/c$ | $U_{iso}$(Å$^2$) |
|---|---|---|---|---|---|---|
| Co | 12*d* | 1 | 0.4291(2) | 0.3525(2) | 0.9551(9) | 0.0067(7) |
| Se(1) | 6*c* | 1 | 0.14830(7) | $-x$ | −.0083(8) | 0.0004(6) |
| Se(2) | 2*b* | 1 | 2/3 | 1/3 | 0.9478(9) | 0.0004(6) |
| O(1) | 6*c* | 1 | 0.2035(6) | $-x$ | 0.216(2) | 0.0025(5) |
| O(2) | 12*d* | 1 | 0.3376(7) | 0.0632(8) | 0.306(1) | 0.0025(5) |
| O(3) | 6*c* | 1 | 0.4017(3) | $-x$ | 0.594(1) | 0.0025(5) |
| O(4) | 6*c* | 1 | 0.4755(5) | $-x$ | 0.134(2) | 0.0025(5) |
| O(5) | 2*a* | 1 | 0.0000 | 0.0000 | 0.114(3) | 0.0025(5) |

$M = Ni^{2+}$; $X = OH^-$

| Cell data | | Reliability factors (%) | |
|---|---|---|---|
| $a = 12.7004(2)$ Å | $V = 687.28(3)$ Å$^3$ | $R_{wp} = 9.80$ | $R_p = 7.06$ $R_B = 4.76$ |
| $c = 4.9201(1)$ Å | $Z = 1$ | $\chi^2 = 5.43$ | |

| Atom | Site | Occupancy | $x/a$ | $y/b$ | $z/c$ | $U_{iso}$(Å$^2$) |
|---|---|---|---|---|---|---|
| Ni | 12*d* | 1 | 0.4316(2) | 0.3543(2) | 0.9721(9) | 0.0140(8) |
| Se(1) | 6*c* | 1 | 0.14743(8) | $-x$ | 0.0117(8) | 0.0021(6) |
| Se(2) | 2*b* | 1 | 2/3 | 1/3 | 0.9599(9) | 0.0021(6) |
| O(1) | 6*c* | 1 | 0.2084(5) | $-x$ | 0.227(2) | 0.005(1) |
| O(2) | 12*d* | 1 | 0.3401(5) | 0.0670(8) | 0.319(1) | 0.005(1) |
| O(3) | 6*c* | 1 | 0.4016(1) | $-x$ | 0.621(1) | 0.005(1) |
| O(4) | 6*c* | 1 | 0.4719(5) | $-x$ | 0.146(2) | 0.005(1) |
| O(5) | 2*a* | 1 | 0.0000 | 0.0000 | 0.115(4) | 0.005(1) |

| $M = Co^{2+}$; $X = F^-$ | $M = Ni^{2+}$; $X = F^-$ |
|---|---|
| Cell parameters | Cell parameters |
| $a = 12.889(4)$ Å $c = 4.985(4)$ Å | $a = 12.702(5)$ Å $c = 4.922(4)$ Å |

*Note.* To obtain more reliable standard deviations, the e.s.d. values in the table must be multiplied by 2.3041 and 3.2145 for the cobalt and nickel hydroxoselenites, respectively (38).

family: $M_{12}Z_nT_8(OH)_6$ ($M$ = transition metal, $T$ = tetrahedral or pseudotetrahedral species, and $Z$ = cationic or anionic species). Each $MO_6$ octahedron shares two edges with other octahedra to form a pyroxene-like $[MO_4]_n$ chain. Face-sharing of two $[MO_4]_n$ chains results in double $[M_4O_{12}]_n$ chains along the $c$ axis. The small triangular channel thus formed is occupied by 2/8 of the selenite groups in the formulas. The remaining $SeO_3^{2-}$ groups connect the $[M_4O_{12}]_n$ chains, forming hexagonal channels that constitute the most interesting feature of these solids. Hence, the framework of these structures, $[M_{12}(SeO_3)_8(OH)_6]^{2+}$, is positively charged.

In the case of the $M_{11}\square(HPO_3)_8(OH)_6$ phosphite derivatives, the excess of positive charge is compensated by random omission of cations in the framework, leading to a 11/12 occupancy factor of the metal sites. In the selenite derivatives, the excess of positive charge is compensated by the presence of additional $OH^-$ or $F^-$ anions in the hexagonal channels. The voids in which the last $OH^-$ anions are located can be described as infinite chains of face-sharing $[E_6]_n$ octahedra ($E$ = lone pair of electrons associated with the Se(IV) cation). The location of the OH groups was confirmed by bond-valence analysis (39, 40).

The hydroxo-fluoro-selenites show X-ray powder diffractograms practically indistinguishable from those of the

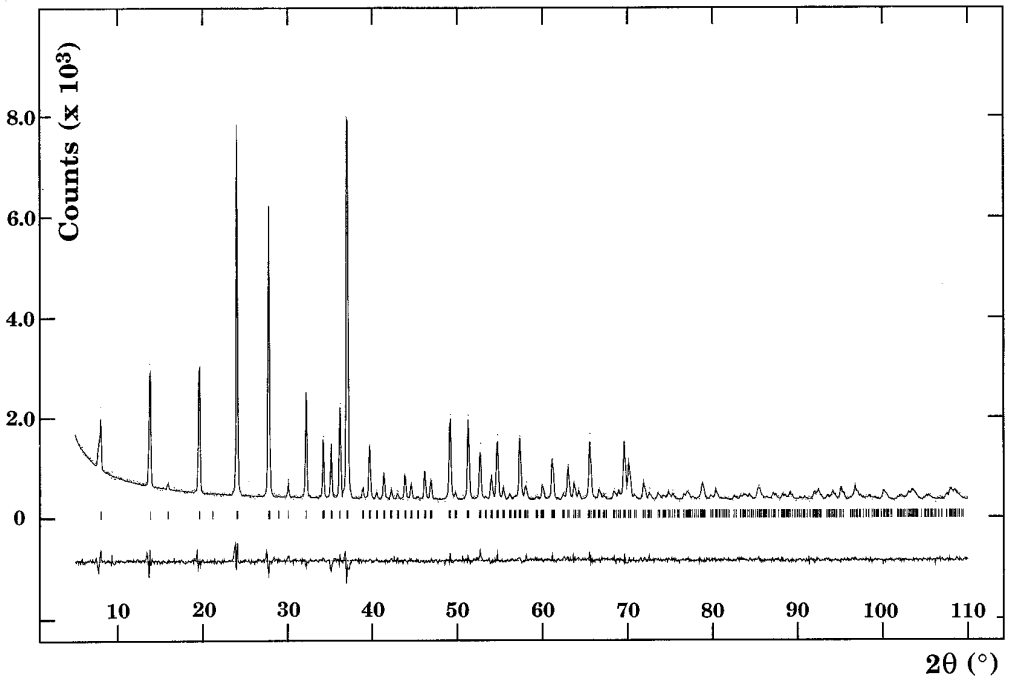


**FIG. 3.** Observed and calculated X-ray powder diffraction patterns of $Co_{12}(OH)_2(SeO_3)_8(OH)_6$. Allowed reflections are marked below the peaks.

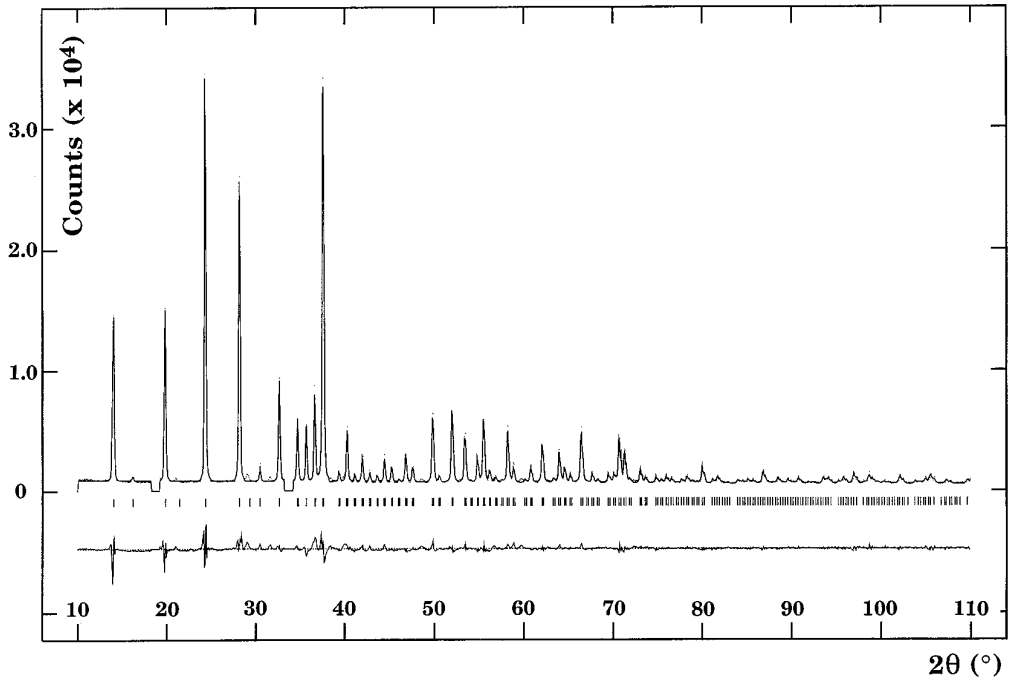


**FIG. 4.** Observed, calculated, and difference profile plots for the Rietveld refinement of the $Ni_{12}(OH)_2(SeO_3)_8(OH)_6$ structure. Allowed reflection positions are indicated by tick marks.

**TABLE 2**
**Selected Bond Distances (Å) and Angles (°) for $M_{12}(OH)_2(SeO_3)_8(OH)_6$ ($M = Co^{2+}$, $Ni^{2+}$)**

| *M*/Se–O | Co | Ni | O–*M*/Se–O | Co | Ni |
|---|---|---|---|---|---|
| *M*–O(1) | 2.154(9) | 2.137(8) | O(1)–*M*–O(4) | 168.7(3) | 167.8(3) |
| *M*–O(2) | 2.043(9) | 2.036(6) | O(1)–*M*–O(4) | 91.0(3) | 87.4(3) |
| *M*–O(2) | 2.068(7) | 2.081(7) | O(1)–*M*–O(3) | 96.2(3) | 95.0(2) |
| *M*–O(3) | 2.062(5) | 2.028(4) | O(1)–*M*–O(2) | 104.1(3) | 104.4(3) |
| *M*–O(4) | 2.154(9) | 2.063(8) | O(1)–*M*–O(2) | 91.6(3) | 93.5(3) |
| *M*–O(4) | 2.176(7) | 2.116(9) | O(3)–*M*–O(2) | 97.15(3) | 95.3(3) |
| | | | O(3)–*M*–O(4) | 80.8(2) | 85.10(2) |
| Se(1)–O(1) | 1.666(6) | 1.709(9) | O(1)–Se(1)–O(2) | 99.1(3) | 96.6(4) |
| Se(1)–O(2) ×2 | 1.707(9) | 1.682(7) | O(1)–Se(1)–O(2) | 99.8(3) | 96.6(3) |
| | | | O(2)–Se(1)–O(2) | 105.8(3) | 100.9(3) |
| Se(2)–O(3) ×3 | 1.691(5) | 1.700(3) | O(3)–Se(2)–O(3) | 102.9(2) | 99.9(1) |

hydroxo-compounds. Their cell parameters are given in Table 1.

The IR spectra (Fig. 6) of $Ni_{12}(OH)_2(SeO_3)_8(OH)_6$ and $Ni_{12}(F)_2(SeO_3)_8(OH)_6$ (cobalt derivative spectra are similar) show two OH stretching bands (at 3520 and 3540 $cm^{-1}$)

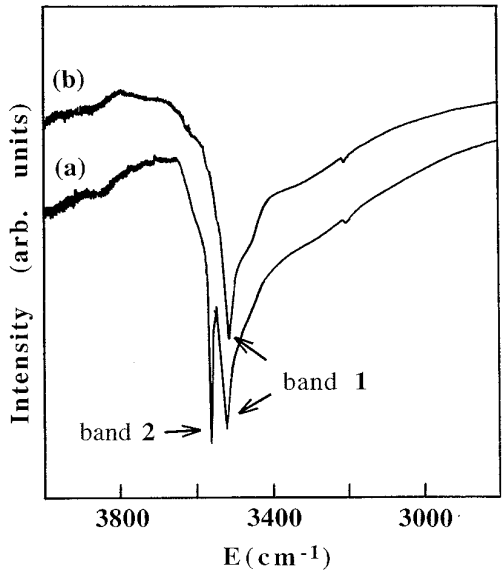


**FIG. 6.** IR spectra (KBr pellet) of solids $Ni_{12}(OH)_2(SeO_3)_8(OH)_6$ **(a)** and $Ni_{12}(F)_2(SeO_3)_8(OH)_6$ **(b)**. Band **1** corresponds to $\upsilon$(O–H) vibration of the O(4)–H hydroxo groups bonded to four metallic atoms. Band **2** is assigned to the $\upsilon$(O–H) vibration of the guest $(O(5)–H)^-$ anions located inside the large hexagonal channel.

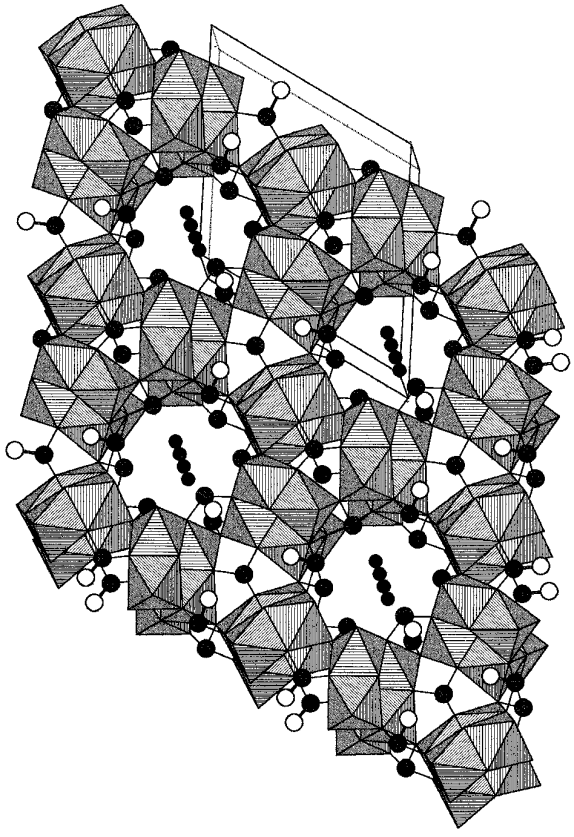

**FIG. 5.** Perspective view of the structure of $M_{12}(OH)_2(SeO_3)_8(OH)_6$ ($M = Co^{2+}, Ni^{2+}$) along the [001] direction. Large filled circles correspond to Se atoms, and the small filled circles to O(5)–H hydroxo groups located in the hexagonal channels. The open circles correspond to oxygen atoms from selenite groups whose metallic polyhedra have not been drawn in the figure.

associated with the two distinct O–H groups, whereas the fluoride derivatives show only one IR absorption band at 3515 $cm^{-1}$. The lower frequency absorption band observed in both fluoride and hydroxide compounds can be assigned to the stretching vibrations of the O(4)–H groups which coordinate the metal atoms in the framework. The band at 3540 $cm^{-1}$ can be attributed to the $OH^-$ guest anions in the hexagonal channels.

Our inability to synthesize such structures with $Cl^-$ or $Br^-$ in the hexagonal channels can be explained from the structural results given here. The trapping of $Z^-$ species is controlled by the dimensions of the hexagonal channels. These channels can be considered as $[E_3]_n$ chains built up from face-sharing $E_6$ octahedra, and trapping of $Z^-$ is controlled by the window defined by the three lone pairs of electrons: 1.58 Å. Only $Z^-$ species having lower ionic radii can be enclosed, as is the case for $OH^-$ (1.37 Å) and $F^-$ (1.33 Å) (41).

Though from an applied point of view thermal stability is a desirable property for porous materials, the selenites described here show only moderate thermal stability when compared to other phosphate or arsenate derivatives of dumortierite (22). For the selenite derivatives, the lower thermal stability of the $SeO_3^{2-}$ anion induces collapse of the structure at *ca.* 400°C. The weight loss begins at 400°C and a very rapid thermal decomposition process is observed in the temperature range 500–560°C.

## ACKNOWLEDGMENTS

We thank very much the Generalitat Valenciana (Grant GV-2227/94) for financial support of this work. M.D.M. thanks the Spanish Ministerio de Educación y Ciencia for a postdoctoral reincorporation contract.

## REFERENCES

1. S. T. Wilson, B. M. Lock, C. A. Messina, T. R. Cannan, and E. M. Flanigen, *J. Am. Chem. Soc.* **104,** 1146 (1982).
2. R. C. Haushalter and L. A. Mundi, *Chem. Mater.* **3,** 31 (1992).
3. J. J. Brezelius, *Acad. Handl. Stockholm* **39,** 13 (1818).
4. J. W. Mellor, ''Comprehensive Treatise on Inorganic and Theoretical Chemistry,'' Vol. 10, pp. 494. Longmans, Green, London, 1965.
5. G. Huan, J. W. Johnson, A. J. Jacobson, and D. P. Goshorn, *Chem. Mater.* **3,** 539 (1991).
6. J. T. Vaughey, W. T. Harrison, L. L. Dussack, and A. J. Jacobson, *Inorg. Chem.* **33,** 4370 (1994).
7. G. Cao, H. Hong, and T. E. Mallouk, *Acc. Chem. Res.* **25,** 420 (1992).
8. K. Kohn, K. Inoue, O. Horie, and S. Akimoto, *J. Solid State Chem.* **18,** 27 (1976).
9. O. J. Lieder, and G. Gattow, *Naturwiss.* **54,** 443 (1967).
10. M. Wildner, *N. Jb. Miner. Monatsh.* **199,** 353 (1990).
11. A. V. P. McManus, W. T. A. Harrison, and A. K. Cheetham, *J. Solid State Chem.* **92,** 253 (1991).
12. M. Wildner, *Monatsh. Chem.* **122,** 585 (1991).
13. W. T. A. Harrison, A. V. P. McManus, and A. K. Cheetham, *Acta Crystallogr. C* **48,** 412 (1992).
14. O. J. Lieder, and G. Gattow, *Naturwiss.* **54,** 318 (1967).
15. M. Wildner, *Acta Crystallogr. C* **48,** 410 (1992).
16. M. Wildner, *J. Solid State Chem.* **115,** 360 (1995).
17. M. D. Marcos, P. Amorós, A. Beltrán, and D. Beltrán, *Solid State Ionics* **63–65,** 87 (1993).
18. M. D. Marcos, P. Amorós, and A. Le Bail, *J. Solid State Chem.* **107,** 250 (1993).
19. M. D. Marcos, P. Amorós, A. Beltrán, R. Martínez, and J. P. Attfield, *Chem. Mater.* **5,** 121 (1993).
20. M. P. Attfield, R. E. Morris, and A. K. Cheetham, *Acta. Crystallogr. C* **50,** 981 (1994).
21. J. L. Pizarro, Ph. D. Thesis, Universidad del Pais Vasco, Lejona, 1990.
22. M. D. Marcos, P. Amorós, D. Beltrán, A. Beltrán, and J. P. Attfield, *J. Mater. Chem.* **5,** 917 (1995).
23. G. Perez, F. Lasserre, J. Moret, and M. Maurin, *J. Solid State Chem.* **7,** 143 (1976).
24. M. D. Marcos, P. Amorós, A. Beltrán, and D. Beltrán, *Solid State Ionics* **63–65,** 96 (1993).
25. P. E. Werner, *Krystallographiya,* **120,** 365 (1969).
26. D. E. Appleman, and H. T. Evans, ''LSUCRE, Indexing and Least Square Refinement of Powder Data,'' N.T.I.S. Document PB-216188.
27. A. C. Larson, and R. B. Von Dreele, Los Alamos National Laboratory Rep. LA-UR-86-748, 1987.
28. C. F. Baes Jr., and R. E. Mesmer, ''The Hydrolysis of Cations.'' Wiley, New York, 1976.
29. A. Stein, S. W. Keller, and T. E. Mallouk, *Science* **259,** 1558 (1993).
30. F. Sapiña, P. Gomez, M. D. Marcos, P. Amorós, R. Ibáñez, D. Beltrán, R. Navarro, C. Rillo, and F. Lera, *Eur. J. Solid State Inorg. Chem.* **26,** 603 (1989).
31. M. D. Marcos, P. Amorós, F. Sapiña, A. Beltrán, R. Martínez, and J. P. Attfield, *Inorg. Chem.* **32,** 5044 (1993).
32. P. Lightfoot, and A. K. Cheetham, *Acta Crystallogr. C* **44,** 1331 (1988).
33. C. F. Baes Jr, and R. E. Mesmer, ''The Hydrolysis of Cations.'' Wiley, New York, 1976.
34. M. J. N. Pourbaix, ''Atlas of Electrochemical Equilibria in Aqueous Solution.'' Pergamon, New York, 1966.
35. M. Wildner, *Acta Crystallogr. C* **50,** 336 (1994).
36. R. J. Hill, and I. C. Madsen, *J. Appl. Crystallogr.* **17,** 297 (1984).
37. R. J. Hill, and I. C. Madsen, *J. Appl. Crystallogr.* **19,** 10 (1986).
38. J. F. Berar, and P. Lelann, *J. Appl. Crystallogr.* **24,** 1 (1991).
39. N. E. Brese, and M. O'Keeffe, *Acta Crystallogr. B* **47,** 192 (1992).
40. I. D. Brown, *Acta Crystallogr. B* **48,** 553 (1992).
41. R. D. Shannon, *Acta Crystallogr. A* **32,** 751 (1976).